

Characterization of octadecaborane implantation into Si using molecular dynamics

Luis A. Marqués,^{*} Lourdes Pelaz, and Iván Santos

Departamento de Electrónica, Universidad de Valladolid, E.T.S.I. de Telecomunicación, 47011 Valladolid, Spain

V. C. Venezia[†]

Axcelis Technologies, Beverly, Massachusetts 01915, USA

(Received 4 October 2006; revised manuscript received 23 October 2006; published 22 November 2006)

We carried out molecular dynamics simulations of monatomic B and octadecaborane cluster implantations into Si. We obtained and analyzed the doping profiles, lateral straggling and the damage amount and morphology produced within the target, as well as its annealing behavior. Our simulation results indicate that the use of octadecaborane clusters for the fabrication of ultrashallow junctions shows several advantages with respect to monatomic B beams, mainly related to target self-amorphization which reduces channeling and the amount of residual damage at the end of range.

DOI: [10.1103/PhysRevB.74.201201](https://doi.org/10.1103/PhysRevB.74.201201)

PACS number(s): 61.43.Bn, 61.72.Cc, 61.72.Tt

Boron ion implantation has traditionally been used for the fabrication of ultrashallow junctions (USJs) in metal-oxide-semiconductor field-effect transistor (MOSFET) devices.¹ But as implant energies are scaled down for each new device generation, monatomic B implantation shows several shortcomings, mainly related to production throughput and ion-beam, high-energy contamination.² The implantation of B clusters has been proposed as an alternative to overcome these drawbacks. The use of decaborane ($B_{10}H_{14}$) has been investigated for more than a decade.³⁻⁵ However, this option has not been viable until very recently due to limitations in the source and vapor delivery systems. These problems have been solved by the development of new implantation equipment² using octadecaborane ($B_{18}H_{22}$) as the source. This molecule delivers on each ion impact almost double the number of B atoms as in the case of decaborane. Recently, promising results have been obtained using this equipment for the fabrication of MOSFET devices with gate lengths of 60 nm.⁶

When manufacturing USJs it is necessary to control not only the dopant profile, but also the damage amount obtained after implantation. The subsequent anneal needed to activate dopants and recombine lattice defects is a highly transient process governed by the diffusion and complex interactions of these two. In particular, interstitial defects produce the so-called B transient enhanced diffusion (TED), which alters junction depth.⁷ The amount of TED depends mainly on the net excess of Si interstitial defects, also known as the “plus factor,” and their proximity to the target surface.^{8,9} For these reasons it is of fundamental importance to fully characterize the damage amount and morphology produced by octadecaborane implantation. Molecular dynamics (MD) is the most appropriate simulation technique to do such characterization. It provides an atomistic description of the implantation process that includes the multiple interactions needed to adequately describe the many-body effects present during cluster implants.¹⁰ While this kind of study has already been carried out for decaborane,^{4,5} this is not the case for octadecaborane.

We carried out MD simulations of monatomic B and octadecaborane cluster implantations into Si in order to make a

comparative study and so determine the advantages and drawbacks of each approach with respect to USJ fabrication. We have paid special attention to the characterization of generated damage. We have used the Tersoff potential^{11,12} to describe the Si-Si, B-B, and Si-B interactions, splined to the universal potential¹³ at short distances to correctly reproduce the high-energy collisions. Since H diffuses out of Si at low temperatures,¹⁴ and in order to have direct comparison with the monatomic B implantations, we have not considered the H atoms in our simulations. Electronic stopping is modeled using a frictional force acting on atoms with energies higher than 10 eV.¹⁵ We solved the classical equations of motion using the fourth-order Gear predictor-corrector algorithm.¹⁶

In our simulations we have used Si targets consisting of 32 000 atoms for monatomic B implantations and 600 000 for B_{18} cluster implantations, at an initial temperature of 0 K. Using these sizes guarantees that the full cascades are contained. Simulation cells are bounded by two (100) planes in the X direction and by four (110) planes in the Y and Z directions. Ions are implanted along the X direction with normal incidence on the (100) Si free surface. The two bottom layers are held fixed and periodic boundary conditions are applied in lateral directions. To have good enough statistics, we have carried out 1000 simulations of monatomic B implants and 56 of B_{18} cluster implants. Ion impact points are randomly chosen along the target surface for monatomic B implants. In the case of cluster implants, B atoms are initially set according to the octadecaborane molecule geometry,¹⁷ with random rotations around the three molecular axes. Every B atom has an initial energy of 500 eV, a typical value used in modern USJ fabrication.⁶ Each implantation event is simulated until the maximum kinetic energy present in the system falls below 0.5 eV, which assures no further damage generation.

To identify the damage resulting from the implantation simulations we have used a method based on the time average of atom coordinates that allows the elimination of thermal vibrations.¹⁸ Averaged configurations are compared with the perfect lattice: if an atom is closer than 0.7 Å to a lattice site, the atom is associated with that site, otherwise it is labeled as “displaced.” Analogously, lattice sites with no associated atom are labeled as “empty.” In order to make a

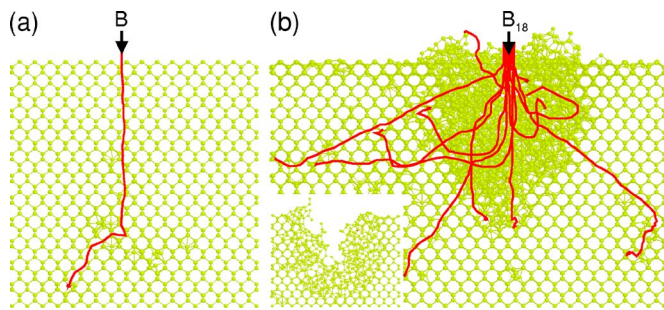


FIG. 1. (Color online) Lateral snapshots showing the typical damage configurations obtained after (a) monatomic B and (b) B_{18} cluster implantations. Solid lines indicate B atom trajectories. Inset in (b) is a 12-Å-thick slice taken around the cluster impact point clearly showing the generated crater.

statistical and morphological study of the damage we have grouped displaced atoms (DAs) and empty lattice sites (ESs) within a first-neighbor distance. Each group of neighboring DAs and ESs forms a *defect complex*, with a size determined by the DA number, and type given by the net number of atoms (DAs minus ESs). Defects with more DAs than ESs are of interstitial (*I*) type, and defects with more ESs than DAs are of vacancy (*V*) type. For example, with this criterion to define damage a single vacancy would be identified as a defect with zero DAs and one ES, a dumbbell interstitial as a defect with two DAs and one ES, and an extended interstitial as a defect with four DAs and three ESs.¹⁸

Figure 1(a) shows the damage created by a typical 500 eV monatomic B cascade. Often the ion gets channeled deep into the target. Damage consists of point defects and small disordered zones, in agreement with MD results obtained by other authors.^{12,19} On average, each monatomic B cascade produces only 32 ± 14 DAs. Figure 1(b) shows the typical damage created by a B_{18} cluster implant. For B_{18} implants, apart from some point defects, there is a large amorphous zone generated around the cluster impact point. The average number of DAs per implanted B atom is 108 ± 8 , more than three times the number obtained in monatomic B implants. A closer look reveals that the amorphous zone is in fact a crater; a large empty volume surrounded by disordered material with the typical rim or hump on the target surface, as can be seen in the inset of Fig. 1(b). It is worth noting that, on average, 70% of the implanted B atoms end up within these amorphous regions around craters.

The obtained B profiles, represented in Fig. 2(a), compare

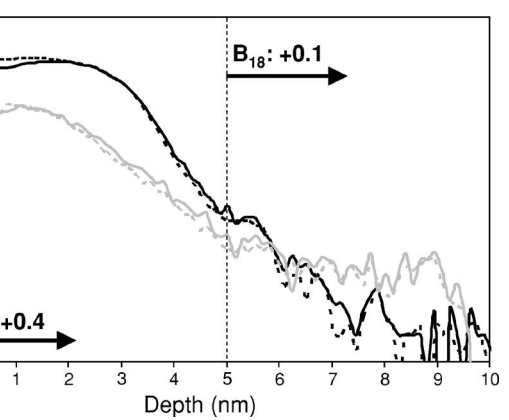
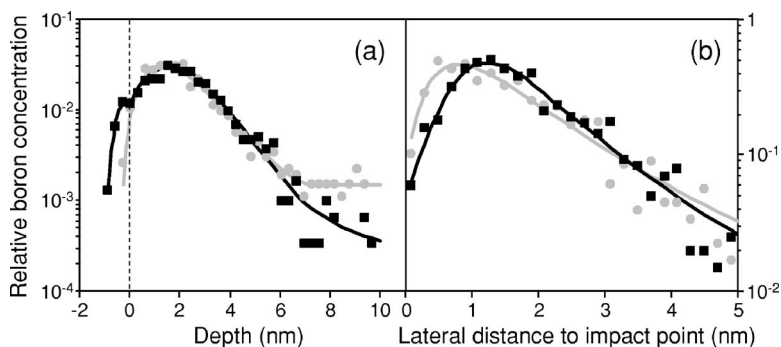


FIG. 3. Relative concentration profiles of DA (solid lines) and ES (dashed lines) per implanted B atom obtained for monatomic (gray) and cluster (black) implantations. Calculated plus factors are also shown.

very well with experiments.⁶ There are two significant differences between the B profiles. The first one is that there are more dopants close to the target surface in the cluster case, due to B atoms that end up attached to crater rims. The second difference appears at the end of range, where B concentration is higher in the monatomic case due to channeling. Self-amorphization produced during cluster implantation minimizes channeling at the expense of increasing the lateral straggling (similar to monatomic B implanted into preamorphized Si), as can be seen in Fig. 2(b). In the monatomic case, the maximum in the lateral straggling profile is around 0.7 nm, while in the cluster case it is almost double that value, 1.3 nm. Nevertheless, the distribution tails are very similar, which implies a steeper lateral profile in the cluster case. This lateral distribution guarantees a proper undergate overlapping of the source and drain regions in MOSFET devices, and the improved abruptness is also beneficial for the sheet-resistance specifications.

Average damage profiles produced per implanted ion are displayed in Fig. 3. In the monatomic case the DA profile is higher than the ES profile, except for the target near-surface zone. This is a direct consequence of how damage is created. As is well known,^{12,19} the B ion produces a cascade where it continuously loses its energy through interactions with the target Si atoms, often generating recoils. Recoils leave small *V* complexes close to the target surface and generate *I* complexes where they stop after completely losing their energy. In the case of B_{18} implantations the total amount of created

FIG. 2. Boron depth profiles (a) and lateral straggling (b) per implanted B atom for monatomic B (gray) and B_{18} (black) implantations. Symbols represent MD data and lines are to guide the eye.

TABLE I. Sputtering (Y_S) and backscattering (Y_B) yields obtained in our MD simulations of B and B₁₈ implants.

| | Y_S | Y_B |
|-----------------|-------|-------|
| B | 0.50 | 0.10 |
| B ₁₈ | 0.85 | 0.08 |

damage is much larger up to a depth of around 5 nm, which corresponds to the formation of amorphous regions around the cluster impact point. There is a net excess of ESs close to the target surface, due to the presence of craters. The large DA amount beyond the surface is a consequence of crater rims. The mechanisms of damage generation are totally different from in the monatomic case and are related to the simultaneous deposition of energy carried by cluster B atoms on the surface region close to the impact point.¹⁰ The temperature in this zone increases above the melting point causing a crystal-to-liquid transition, similar to the one observed in heavy-ion implantations.¹⁹ Four picoseconds after cluster impact the liquid core starts transforming into amorphous material due to the fast temperature drop caused by heat dissipation throughout the target. This thermal spike regime also produces a significant enhancement in the sputtering yield (see Table I) due to surface destabilization as a consequence of the temperature increase. However, it is noteworthy that at depths above 7 nm there is more damage in the monatomic case, related to channeled boron.

Figure 4 shows the relative appearance frequency of each defect type, characterized by its size (number of DAs) and its net number of atoms. In the monatomic case damage is in the form of small point defects (number of DAs below 10), most of which are single self-interstitials and small bond defect complexes²⁰ without an excess or deficit of atoms with respect to the perfect lattice. There are also single vacancies and di-interstitials, but these appear much less frequently. In the case of cluster implantations, most DAs are in large defect complexes with a size around 2000. These DA complexes are the craters created by the cluster ion impact, which appear as large *V* defects due to our method of identifying damage. There are also a few point defects, which are generated by B atoms and recoils that escape from the amorphous zones surrounding craters.

From the statistical analysis of damage obtained in B₁₈ cluster implants we have estimated the extension of the amorphous layer that would be created with typical implantation parameters. Amorphous zones surrounding craters are cylindrical with an average diameter of 4 nm from the surface to a depth of 3 nm, and conical from 3 nm to around 5 nm below the surface [see Fig. 1(b)]. Taking into account that each cluster delivers 18 B atoms, the estimated equivalent B dose to fully amorphize the target surface is $1.4 \times 10^{14} \text{ cm}^{-2}$, which is 70 times lower than the dose needed in monatomic B implantation.¹ The created amorphous layer would be around 3 nm thick. For a dose of 10^{15} cm^{-2} , a value routinely used to fabricate USJs, the amorphous layer would extend up to a depth of 5 nm.

Typical annealing conditions cannot be directly simulated using MD techniques since the required time scales are not

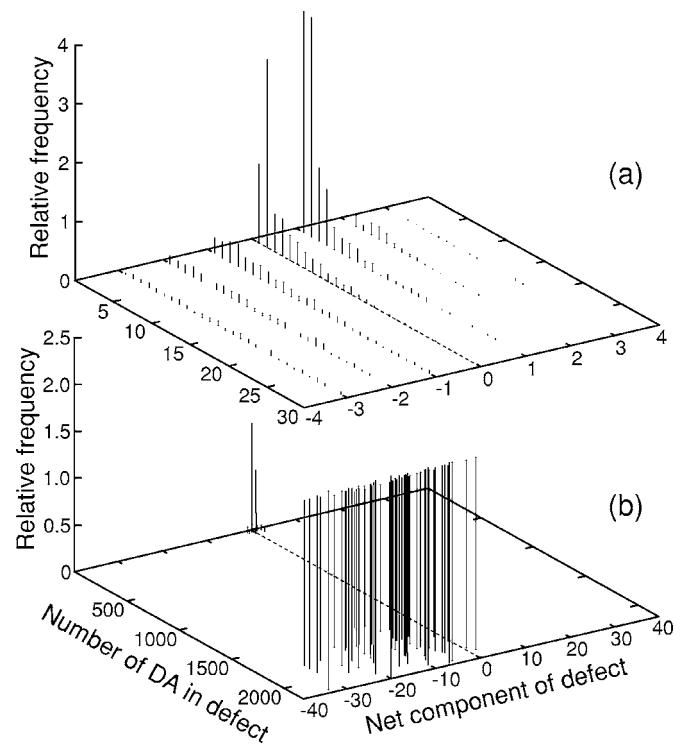


FIG. 4. Relative frequency of appearance of each defect complex type, as a function of its number of DAs and its net number of atoms, for (a) monatomic and (b) cluster implantations. The sum of all frequencies gives the average number of DAs per implanted B atom. Defects on the right of the dashed line are *I*-type and *V*-type complexes on the left.

affordable. However, annealing simulations can be performed by setting the temperature as high as possible to accelerate system dynamics ($T=2200 \text{ K}$, 200 K below the melting temperature within the Tersoff model of Si). As an example, in Fig. 5 we show three snapshots taken during the damage annealing obtained after a B₁₈ implant simulation. The underlying crystal substrate serves as a seed for the recrystallization process. At the end, the amorphous region has recrystallized completely, the crater and the rim have disappeared. Only point defects outside the initial amorphous zone remain after annealing. B atoms inside the amorphous zone are not swept by the amorphous/crystal interface, and eventually are incorporated into substitutional positions. In the case of damage created by monatomic B, only bond defect complexes disappear during the same annealing conditions. The remaining point defects, single self-interstitials, di-interstitials and single vacancies, which are highly mobile species, will recombine with each other leaving behind only the excess Si interstitials near the end-of-range region.

The amount of TED that would be obtained during thermal treatments can be estimated by the plus factor calculation, defined as the total net component of defect complexes inside the target, DA profile minus ES profile of Fig. 3. For a typical B dose of 10^{15} cm^{-2} amorphization does not occur in the monatomic case, and the plus factor is given by the integral of the net damage from the surface. The obtained value is +0.4, consistent with the +1 model²¹ ($1 - Y_S - Y_B$). Boron and self-interstitials coexist in the same region which

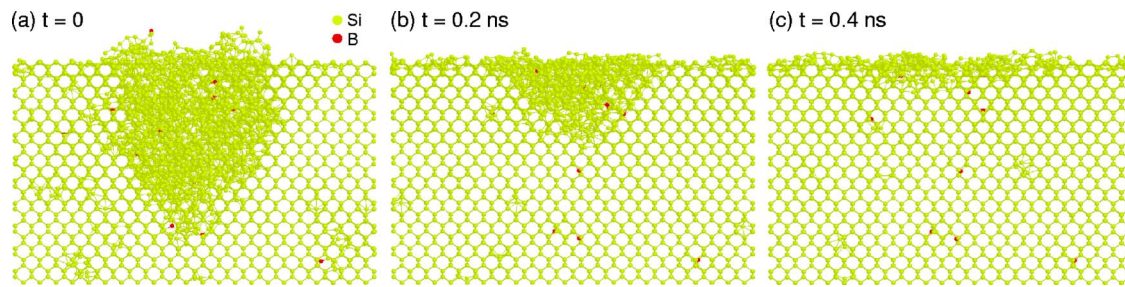


FIG. 5. (Color online) Lateral snapshots taken during annealing at $T=2200$ K of one of the samples implanted with a B_{18} cluster.

favors the formation of B-I clusters responsible for electrical deactivation.²² The complete reactivation requires a high thermal budget which is accompanied by significant diffusion. Preamorphization followed by solid-phase epitaxial regrowth provides a better activation with lower thermal budgets.²³ In the cluster implantation case, a 5 nm continuous amorphous layer is formed. Its recrystallization leaves no defects below the initial amorphous/crystal interface position, and the plus factor is calculated by the integral of the damage from that position. The obtained plus factor is only +0.1, indicating less TED than in the monatomic case. In addition, cluster implants can take advantage of the higher activation level during solid-phase epitaxial regrowth without the need of a preamorphization implant step. These are promising results, although it is necessary to point out that they have to be considered in the framework of our simulations, where some approximations have been assumed: the

use of semiempirical potentials to describe atomic interactions, the fact that H atoms have been ignored, and also that annealings have been carried out at very high temperatures.

In conclusion, we carried out MD simulations of monatomic B and B_{18} cluster implantations into Si. We obtained the profiles of generated damage, implanted boron, and lateral straggling, and analyzed the mechanisms of damage formation and annealing. We demonstrated that the use of B_{18} clusters to fabricate USJs shows several advantages with respect to monatomic B beams, such as self-amorphization which reduces channeling and improves activation. The formed amorphous layer is very shallow and therefore the remaining end-of-range defects are very close to the surface, which requires lower thermal budgets for their anneal.

This work has been supported by the Spanish DGI under Project No. TEC2005-05101 and the JCYL Consejería de Educación y Cultura under Project No. VA070A05.

*Electronic address: lmarques@ele.uva.es

†Present address: OmniVision Technologies, Inc., Sunnyvale, CA 94089.

¹K. S. Jones, D. K. Sadana, S. Prussin, J. Washburn, E. R. Weber, and W. J. Hamilton, *J. Appl. Phys.* **63**, 1414 (1988).

²D. Jacobson, T. Horsky, W. Krull, and B. Milgate, *Nucl. Instrum. Methods Phys. Res. B* **237**, 406 (2005).

³D. Takeuchi, H. Shimada, J. Matsuo, and I. Yamada, *Nucl. Instrum. Methods Phys. Res. B* **121**, 345 (1997).

⁴R. Smith, M. Shaw, R. P. Webb, and M. A. Foad, *J. Appl. Phys.* **83**, 3148 (1998).

⁵T. Aoki, J. Matsuo, G. Takaoka, N. Toyoda, and I. Yamada, *Nucl. Instrum. Methods Phys. Res. B* **206**, 855 (2003).

⁶Y. Kawasaki *et al.*, *Nucl. Instrum. Methods Phys. Res. B* **237**, 25 (2005).

⁷Y. F. Chong, K. L. Pey, A. T. S. Wee, A. See, L. Chan, Y. F. Lu, W. D. Song, and L. H. Chua, *Appl. Phys. Lett.* **76**, 3197 (2000).

⁸L. Pelaz, G. H. Gilmer, M. Jaraiz, S. B. Herner, H.-J. Gossmann, D. J. Eaglesham, G. Hobler, C. S. Rafferty, and J. Barbolla, *Appl. Phys. Lett.* **73**, 1421 (1998).

⁹L. Pelaz, G. H. Gilmer, V. C. Venezia, H.-J. Gossmann, M. Jaraiz, and J. Barbolla, *Appl. Phys. Lett.* **74**, 2017 (1999).

¹⁰S. Ihara, S. Itoh, and J. Kitakami, *Phys. Rev. B* **58**, 10736 (1998).

¹¹J. Tersoff, *Phys. Rev. B* **39**, 5566 (1989).

¹²A. M. C. Pérez-Martín, J. J. Jiménez-Rodríguez, and J. C. Jiménez-Sáez, *Nucl. Instrum. Methods Phys. Res. B* **234**, 228 (2004).

¹³J. F. Ziegler, J. P. Biersack, and U. Littmark, *The Stopping and Range of Ions in Solids* (Pergamon, New York, 1985).

¹⁴J. Wong-Leung, C. E. Ascheron, M. Petravic, R. G. Elliman, and J. S. Williams, *Appl. Phys. Lett.* **66**, 1231 (1995).

¹⁵M. Hedström and H.-P. Cheng, *Phys. Rev. B* **59**, 10701 (1999).

¹⁶C. W. Gear, *Numerical Initial Value Problems in Ordinary Differential Equations* (Prentice-Hall, Englewood Cliffs, NJ, 1971).

¹⁷P. G. Simpson and W. N. Lipscomb, *Proc. Natl. Acad. Sci. U.S.A.* **48**, 1490 (1962).

¹⁸L. A. Marqués, L. Pelaz, P. Castrillo, and J. Barbolla, *Phys. Rev. B* **71**, 085204 (2005).

¹⁹M.-J. Caturla, T. Diaz de la Rubia, L. A. Marqués, and G. H. Gilmer, *Phys. Rev. B* **54**, 16683 (1996).

²⁰L. A. Marqués, L. Pelaz, J. Hernández, J. Barbolla, and G. H. Gilmer, *Phys. Rev. B* **64**, 045214 (2001).

²¹M. Giles, *J. Electrochem. Soc.* **138**, 1160 (1991).

²²L. Pelaz, G. H. Gilmer, H.-J. Gossmann, C. S. Rafferty, M. Jaraiz, and J. Barbolla, *Appl. Phys. Lett.* **74**, 3657 (1999).

²³S. Solmi, E. Landi, and F. Baruffaldi, *J. Appl. Phys.* **68**, 3250 (1990).